liquid that moves, it is much easier to think of the motion of the bubble in the opposite direction.

In a semiconductor having bandgap energy E_g, the (conduction) electron density n and the hole density p have the following relationship:

$$np = Be^{-E_g/kT} \equiv n_i^2 \tag{3.2.1}$$

where B is more or less a constant for all semiconductors ($B \approx 10^{39}$ cm^{-6}), k is the Boltzmann constant, and T is temperature in degrees Kelvin. In pure, or *intrinsic* semiconductors, n and p are equal and

$$n = p = n_i \tag{3.2.2}$$

Therefore n_i is known as the *intrinsic carrier concentration*. Table 10.2 shows the E_g of some selected semiconductors.

For Si, with $E_g = 1.12$ eV, n_i is only about 10^{10} cm^{-3} at room temperature. When one considers that metals have $n > 10^{22}$ cm^{-3} it is clear that pure silicon is relatively nonconductive. The conductivity of Si may be increased by adding a small amount of group V elements such as P or As, as shown in Fig. 3.2*b*. After contributing four electrons to fulfill the covalent bonds, P has a fifth electron that can then easily escape from the P nucleus and become a free electron. Such impurity atoms are called *donors*, since they donate electrons. If the donor density N_d is much larger than n_i,

$$n = N_d \tag{3.2.3}$$

and

$$p = n_i^2/n = n_i^2/N_d \tag{3.2.4}$$

For example, a Si sample doped with 10^{15} cm^{-3} of P would have $n = 10^{15}$ cm^{-3} and $p = 10^5$ cm^{-3}. Notice that $n >> p$ in donor-doped semiconductors, which are called n-type semiconductors. Here electrons are the *majority* carriers and holes are the *minority* carriers.

Similarly, if group III elements such as B or Al are added into Si, holes are created. Such dopant atoms are called *acceptors* since they accept additional electrons; and semiconductors doped with acceptors are called p-type semiconductors. If N_a is the acceptor density,

$$p = N_a \tag{3.2.5}$$

and

$$n = n_i^2/N_a \tag{3.2.6}$$

In p-type semiconductors, $p >> n$. Holes are the majority carriers and electrons are the minority carriers.

The above discussion also applies to Ge, another group IV semiconductor. For another example, Fig. 3.2*c* shows the atomic arrangement of

gallium arsenide. Ga is a group III element and As is a group V element. The most common donors of GaAs are group VI elements such as S, which substitutes for As. The most common acceptors of GaAs are group II elements such as Te, which substitutes for Ga. Si, a group IV element, can be either a donor or an acceptor in GaAs, depending on whether it substitutes for Ga or As, which in turn depends on the temperature at which Si is introduced into GaAs.

The electrical conductivity σ of a semiconductor is

$$\sigma = q\mu_n n + q\mu_p p \tag{3.2.7}$$

where μ_n and μ_p are the electron and hole mobilities, which are two characteristic parameters of the semiconductor and, for a given semiconductor, are somewhat dependent on doping density and temperature. The conductivity is roughly proportional to the majority carrier density. Figure 3.3 shows the conductivities of p- and n-type Si. It is common to specify the dopant type and conductivity of a sample. From Fig. 3.3, the dopant density can be found.

One often encounters a graphical representation of semiconductors known as the *energy-band diagram*. The upper line in Fig. 3.4*a* is the conduction-band edge, representing the lowest energy that conduction electrons may have. The lower line is the valence-band edge or the lowest energy that holes can have. The two lines are, of course, separated by the bandgap energy E_g. Most electrons have energies within a few kT above the conduction-band edge. Most holes have energies within a few kT below the valence-band edge. Seeking the lowest energy point, an electron moves downward and a hole moves upward in the energy-band diagram—a fact that happens to fit the bubble analogy of holes well.

Since the conduction-band edge represents the energy of an electron at rest (zero kinetic energy), it must reflect the variation of electric potential. In Fig. 3.4*b*, the left end of the sample is at a potential (defined by convention for a positive charge) 2 volts higher than the right end. The *electron* potential energy then is 2 eV *lower* at the left end. The consistency of the pictures presented so far may be verified by one observation. The voltage source in Fig. 3.4*b* creates a field pointing to the right in the sample. Electrons would be accelerated to the left and holes to the right. This means that electrons move downhill and holes move uphill in the accompanying energy diagram, as expected.

3.3 LIGHT ABSORPTION AND CARRIER GENERATION

Each semiconductor is characterized by a bandgap energy E_g, the energy needed to free an electron from the nucleus and thus create one electron-hole pair. This energy can be supplied in the form of light. Each light photon has energy $h\nu$, where h is the Planck's constant and ν is the frequency of the light

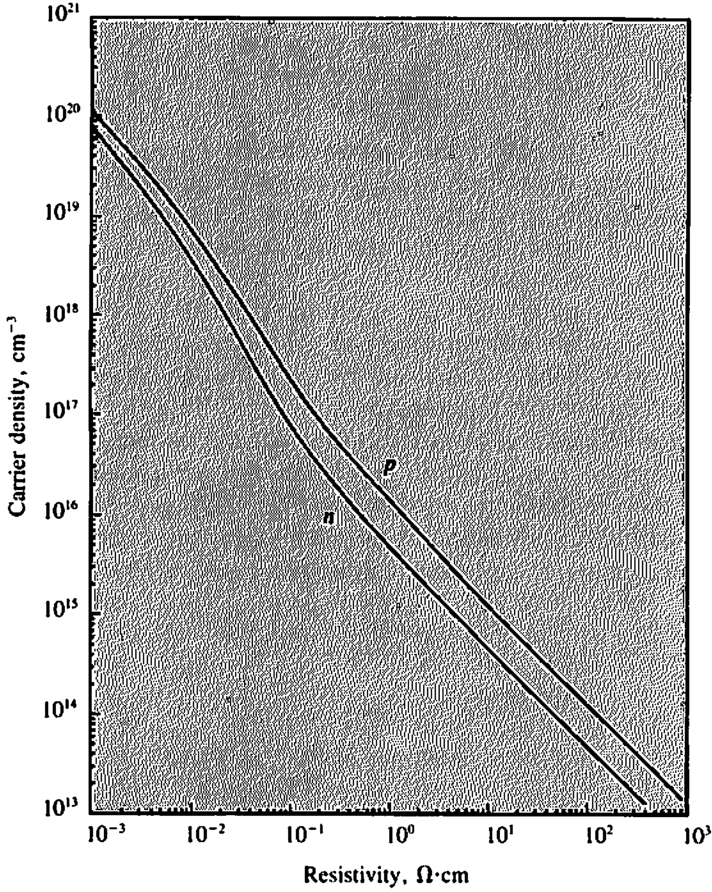

Figure 3.3 Room temperature conductivities of n- and p-type Si as functions of doping density.

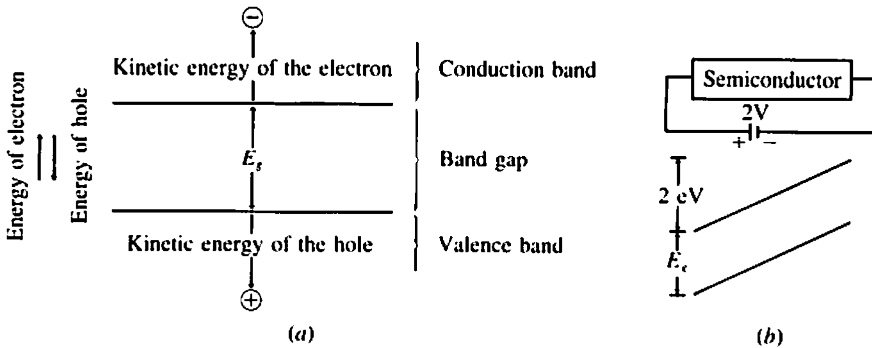

Figure 3.4 (a) Important concepts associated with the energy-band diagram. (b) The energy-band diagram reflects the electric potential variations in the sample.

wave. The energy $h\nu$ can be expressed as

$$h\nu(\text{eV}) = h\frac{c}{\lambda} = \frac{1.24}{\lambda(\mu\text{m})} \tag{3.3.1}$$

where c is the speed of light and λ is the light wavelength. For example, each light photon of 0.62 μm wavelength has 2 eV energy. Semiconductors can absorb photons having $h\nu > E_g$. The energy of each absorbed photon is consumed by raising a valence-band electron into the conduction band and creating one electron and one hole.

Each photon having $h\nu$ greater than E_g (up to several E_g) is capable of generating one and only one electron-hole pair. The excess energy is dissipated as heat. Photons with $h\nu < E_g$ are basically not absorbed by the semiconductor and cannot generate electron-hole pairs. This fact plus the spectral distribution of solar radiation lead to the conclusion that the maximum photon-absorption rate or carrier-generation rate per unit area is a function of E_g of the semiconductor, as shown in Fig. 3.5. Figure 3.5 is also a plot of the cell-current density assuming that all the light-generated carriers contribute to the cell current. The actual carrier-generation rate may be less

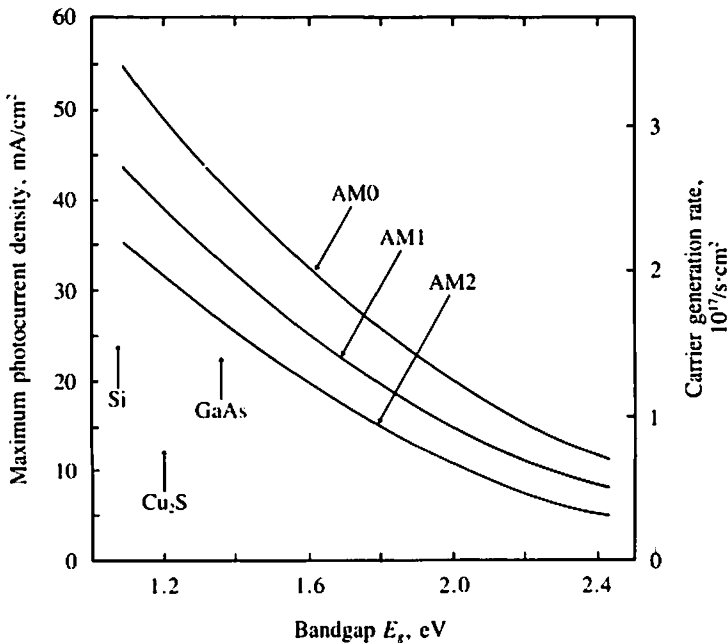

Figure 3.5 The carrier-generation rate and the maximum available cell current per unit area of cell as a function of the bandgap energy of the cell material. (See Chap. 2 for explanation of the air mass number.)

because of, for example, light reflection at the cell surface; and the actual cell current may be yet less because of incomplete collection of the carriers, as discussed in Sec. 3.6. The important fact is that cells made of narrow bandgap (small E_g) materials can be expected to generate more current.

There is a more subtle aspect to light absorption. Photons are not absorbed immediately upon incidence on the semiconductor surface. Rather, some photons can travel a considerable distance in the semiconductor before being absorbed. In general the photon flux, number of photons per square centimeter per second, decreases exponentially with the distance of travel x

$$F(x) = F(0)e^{-\alpha x} \tag{3.3.2}$$

Therefore, the rate of photon absorption and hence the rate of carrier generation per unit volume is

$$G(x) = \frac{-dF(x)}{dx} = \alpha F(0)e^{-\alpha x} \tag{3.3.3}$$

α is called the *absorption coefficient* and is the inverse of the average photon penetration depth. As shown in Fig. 3.6, α is a function of λ or $h\nu$. α is

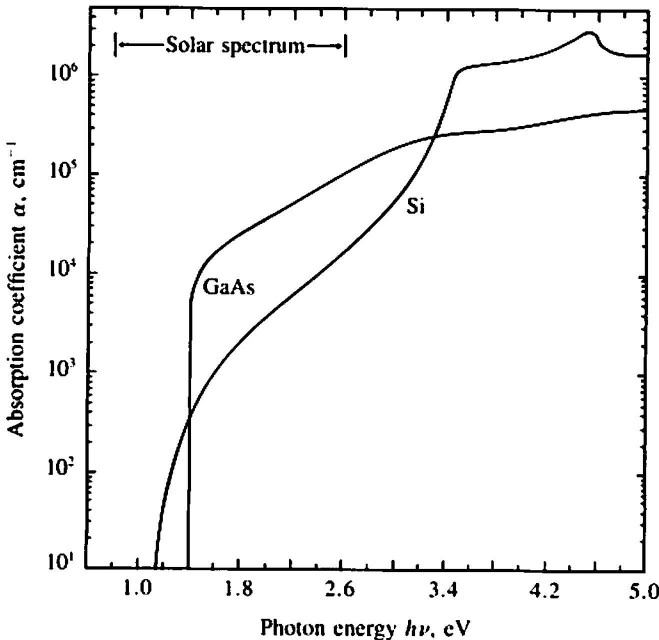

Figure 3.6 Light absorption coefficient as a function of photon energy. Si and GaAs typify the indirect- and direct-gap semiconductors.

essentially zero for $h\nu < E_g$* and larger than 10^4 cm^{-1} for large $h\nu$. In the GaAs case, this transition in α occurs rather abruptly; in Si, it occurs gradually. An abrupt change in α from 0 for $h\nu < E_g$ to a value larger than 10^4 cm^{-1} for $h\nu > E_g$ is characteristic of a class of semiconductors called the *direct-gap* semiconductors. Besides GaAs, this group includes InP, CdS, and Cu_2S. The behavior of Si is characteristic of the other group called the *indirect-gap* semiconductors, including Ge and GaP. It is difficult to predict whether a semiconductor is of the direct-gap type or the indirect-gap type since the difference is caused by the different electronic structures of the semiconductor crystals in a complicated way.

The effects are clear. Figure 3.7 shows that Si, an indirect-gap semiconductor, cannot absorb nearly all the photons with $h\nu > E_g$ until the sample is at least 100 μm thick. By contrast, GaAs, a direct-gap semiconductor, can do so with a sample 1 μm thick. Direct-gap semiconductors, then, are more suitable materials for "thin-film" solar cells. In general, less (thinner) direct-gap semiconductor material is required for making solar cells than is indirect-gap semiconductor material. This may be an important consideration in the selection of solar cell materials.

3.4 CARRIER RECOMBINATION

Echoes in a canyon eventually die out; water stirred by a cast stone will regain its calm. Nature provides means for things to return to their equilibrium states. If the carrier concentrations are made to exceed their *equilibrium* values given in Eqs. (3.2.3) to (3.2.6), such as by photo-carrier generation, the excess carriers die away by *recombination*. The rate at which *excess* electrons and holes recombine and annihilate each other in pairs is

$$\text{Recombination rate, per volume per second} = \frac{n - n_0}{\tau} = \frac{p - p_0}{\tau} \, (\text{cm}^{-3}\text{s}^{-1}) \tag{3.4.1}$$

n_0 and p_0 are the equilibrium electron and hole densities; τ is the *recombination lifetime* or simply the *lifetime* of the carriers.

Long lifetimes are desirable if not essential for achieving high solar cell efficiencies. In direct-gap semiconductors of moderately high doping densities, the dominant recombination mechanism is usually the band-to-band recombination illustrated in Fig. 3.8*a*. Clearly, the higher the majority carrier concentration, the higher the probability of electrons' meeting and recombining with holes; thus one finds

* Measuring the edge of the absorption spectrum is in fact the most common way of finding the E_g of a semiconductor.

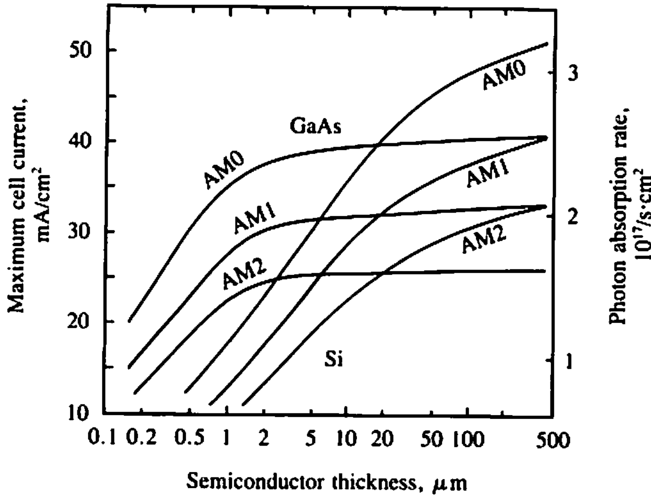

Figure 3.7 Maximum available cell current density and rate of photon absorption as function of cell thickness.

$$\tau_{\text{band-band}} = \frac{C}{\text{doping density}} \qquad (3.4.2)$$

This recombination mechanism is the reverse of photon absorption. It is therefore more likely in direct-gap semiconductors, for which $C \approx 10^{10}$ $\text{s} \cdot \text{cm}^{-3}$, than in indirect-gap semiconductors, for which $C \approx 10^{15}$ $\text{s} \cdot \text{cm}^{-3}$ (Varshni, 1967).

Figure 3.8*b* illustrates the Auger recombination. Since two majority carriers are involved,

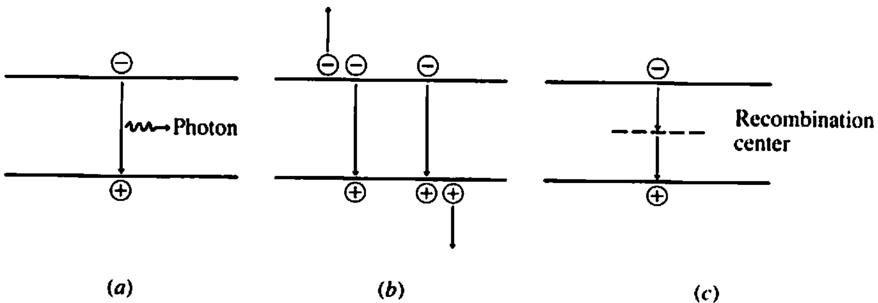

Figure 3.8 Important recombination mechanisms: (*a*) Band-to-band recombination is the reverse of photon absorption and important in direct-gap semiconductors. (*b*) Auger recombination is dominant in heavily doped semiconductors. (*c*) Recombination through traps is dominant in lightly doped Si.

$$\tau_{\text{Auger}} = \frac{D}{(\text{doping density})^2} \tag{3.4.3}$$

Auger recombination may be dominant in most heavily doped semiconductors.

For lightly doped semiconductors, recombination through recombination *centers* (also known as *deep levels* or *traps*) may dominate. This is illustrated in Fig. 3.8*c*. In such materials,

$$\tau_{\text{trap}} = \frac{1}{v\sigma_T N_T} \tag{3.4.4}$$

where v is the thermal velocity of the carriers, σ_T is the capture cross-section of the traps, and N_T is the trap concentration. Some chemical impurities in Si such as gold and platinum have large σ_T and therefore must be avoided in solar cells. Many semiconductor processing steps can create crystal imperfections (see Chap. 4), which behave as traps. It is possible for a silicon sample having a lifetime as long as several hundred microseconds at the beginning of the solar cell fabrication process to emerge at the end of the process with a lifetime shorter than one microsecond.

Finally, since the total recombination rate is the sum of the three separate recombination rates,

$$\frac{1}{\tau} = \frac{1}{\tau_{\text{band-band}}} + \frac{1}{\tau_{\text{Auger}}} + \frac{1}{\tau_{\text{trap}}} \tag{3.4.5}$$

Figure 3.9 shows that recombination lifetime can vary randomly over a large range due to unintentionally introduced recombination centers. The only predictable trend is that carrier lifetimes tend to fall off at high doping densities, presumably due to Auger recombination and, in the case of direct-gap semiconductors, band-to-band recombination.

Another concept closely related to recombination lifetime is diffusion length. Suppose there is a steady source of carrier generation at one plane in a sample; the minority carriers will diffuse away from the plane while recombination diminishes their numbers. The result is an excess-carrier-density profile that decreases exponentially with distance from the plane with a decay length called the *diffusion length*, L (Muller and Kamins, 1977),

$$L = \sqrt{kT\mu\tau/q} = \sqrt{D\tau}, \tag{3.4.6}$$

where $D = kT\mu/q$ is the *diffusion coefficient*. Usually L and D are accompanied with subscripts n or p to denote whether electrons or holes are being considered.

3.5 *pn* JUNCTIONS

All practical photovoltaic cells have intentionally built-in asymmetry, i.e., one side of the cell is different from the other side. Without some asymmetry,

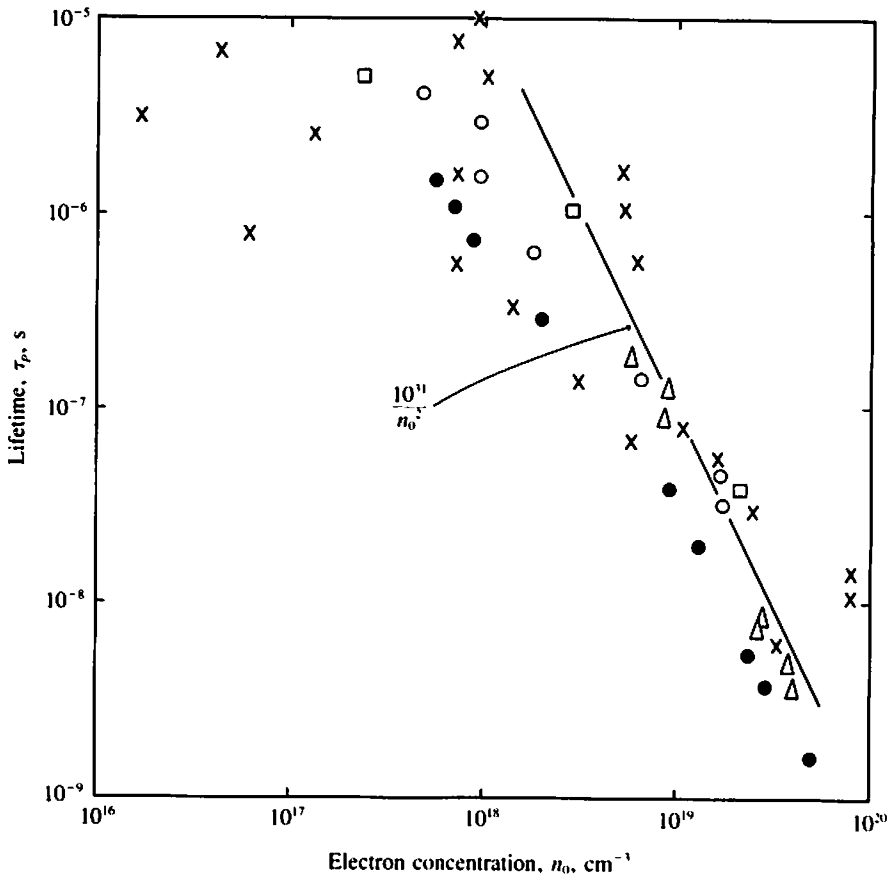

Figure 3.9 Recombination lifetime in n-type Si measured by different investigators (indicated by different symbols). At high doping densities, the lifetimes fit Eq. (3.4.3) with $D = 10^{31}\text{s} \cdot \text{cm}^{-6}$. τ_n has similar dependence on p_0.

there would be no reason for current to flow in one direction rather than the other (assuming uniform illumination in both directions) and the only reconciliation would be that no current flows in either direction. When the asymmetry consists of a p-type semiconductor on one side and an n-type semiconductor on the other, as shown in Fig. 3.10*a*, the structure is known as a *pn junction*. In this section, we shall discuss unilluminated *pn* junctions and remark on the general properties of some other junction structures of interest.

Due to the differences in electron and hole concentrations on the two sides, there is a strong tendency for electrons to diffuse from the n side to the p side and for holes to diffuse in the opposite direction. Such diffusions would cause positive charges to appear on the n side and negative charges to appear on the p side (Fig. 3.10*a*). The resultant double layer of charges sets up an electric field. The field in turn creates an internal potential drop at the junc-

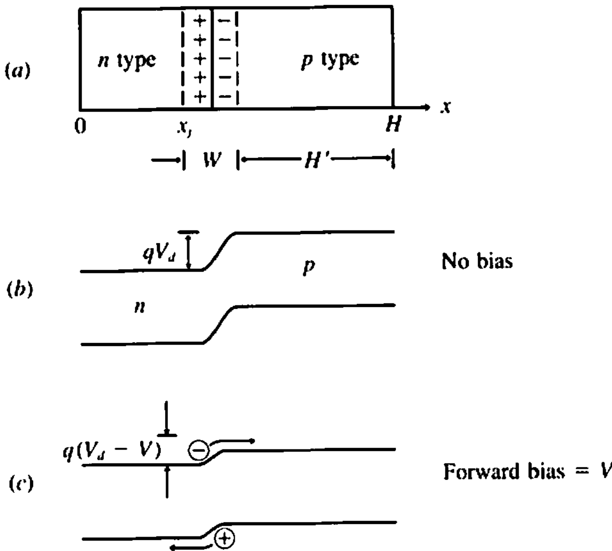

Figure 3.10 (*a*) *pn* junction. (*b*) and (*c*) Energy-band diagrams with no voltage and with V applied across the junction.

tion. This condition is illustrated in Fig. 3.10*b* by the use of an energy diagram. The tendency of the electrons to diffuse to the right is balanced by their tendency to move downward in an energy diagram (see Sec. 3.2) or to be stopped by a potential barrier. To exactly counterbalance the diffusion tendency, the built-in voltage can be shown to be (Muller and Kamins, 1977)

$$V_d = \frac{kT}{q} \ln \frac{N_d N_a}{n_i^2} \tag{3.5.1}$$

The space containing the two charge layers is called the *depletion region* or the *space-charge region*.

When a bias voltage is applied to the junction with the p side positive with respect to the n side, the pn junction is *forward-biased* and the energy diagram is as shown in Fig. 3.10*c*. The potential barrier is not high enough to balance the diffusion tendency and electrons are *injected* into the p side and holes *injected* into the n side with a resultant current flow. For reference and without proof or discussion, we now list the basic equations (Muller and Kamins, 1977, or Grove, 1967, or any textbook on semiconductor electronics) that govern the behaviors of the minority carriers. (See Fig. 3.10*a* for the geometry of the junction.)

$$\frac{dJ_n}{dx} - \frac{n_p - n_{p0}}{q\tau_n} = 0 \tag{3.5.2}$$

$$J_n = q\mu_n n_p E + qD_n \frac{dn_p}{dx} \tag{3.5.3}$$

(Eqs. 3.5.2 and 3.5.3: electrons on p side)

$$\left.\begin{aligned} &\frac{dJ_p}{dx} + \frac{p_n - p_{n0}}{q\tau_p} = 0 \\ &J_p = q\mu_p p_n E - qD_p \frac{dp_n}{dx} \end{aligned}\right\} \text{holes on } n \text{ side} \qquad \begin{aligned}(3.5.4)\\(3.5.5)\end{aligned}$$

The boundary conditions are

$$p_n = p_{n0} e^{qV/kT} \qquad x = x_j \tag{3.5.6}$$

$$n_p = n_{p0} e^{qV/kT} \qquad x = x_j + W \tag{3.5.7}$$

$$S_p(p_n - p_{n0}) = D_p \frac{dp_n}{dx} - \mu_p p_n E_p \qquad x = 0 \tag{3.5.8}$$

$$S_n(n_p - n_{p0}) = -D_n \frac{dn_p}{dx} - \mu_n n_p E_n \qquad x = H \tag{3.5.9}$$

J is the current density, μ is the mobility, S is the surface recombination velocity, and $D = kT\mu/q$ is the diffusion coefficient. The subscripts n and p indicate electrons or holes except for n_p and p_n, which are the electron concentration on the p side and the hole concentration on the n side, respectively. The subscript 0 stands for equilibrium.

If the doping levels on the two sides are uniform, then the electric fields outside the depletion region, E_n and E_p, are negligible and the solution to Eqs. (3.5.2) through (3.5.5) is

$$p_n - p_{n0} = C_1 \cosh\frac{x}{L_p} + C_2 \sinh\frac{x}{L_p} \qquad x \le x_j \tag{3.5.10}$$

$$n_p - n_{p0} = C_3 \cosh\frac{x}{L_n} + C_4 \sinh\frac{x}{L_n} \qquad x_j + W \le x \le H \tag{3.5.11}$$

Using the boundary conditions of Eqs. (3.5.6) through (3.5.9), C_1 through C_4 can be found and the injected current density (A/cm^2) is

$$J_{\text{inj}} = J_0 (e^{qV/kT} - 1) \tag{3.5.12}$$

$$J_0 = q\frac{D_p}{L_p}\frac{n_i^2}{N_d} \frac{\frac{S_pL_p}{D_p}\cosh\frac{x_j}{L_p} + \sinh\frac{x_j}{L_p}}{\frac{S_pL_p}{D_p}\sinh\frac{x_j}{L_p} + \cosh\frac{x_j}{L_p}} + q\frac{D_n}{L_n}\frac{n_i^2}{N_a} \frac{\frac{S_nL_n}{D_n}\cosh\frac{H'}{L_n} + \sinh\frac{H'}{L_n}}{\frac{S_nL_n}{D_n}\sinh\frac{H'}{L_n} + \cosh\frac{H'}{L_n}} \tag{3.5.13}$$

J_0 is known as the *reverse saturation current* of the junction. We shall see later that it is desirable to minimize J_0 of a solar cell. It is only necessary to

remember from Eq. (3.5.13) that the first term represents hole injection into the n region and that, to minimize it, N_d and L_p should be made large and S_p small (few recombinations at the front surface). The second term represents electron injection into the p region and can be reduced by making N_a and L_n large and S_n small. Even for arbitrary and nonuniform N_a, N_d, E, τ, and D, Eq. (3.5.12) is still valid; however, it is impossible to express J_0 in a closed form in the general case.

While the current represented by Eq. (3.5.12) is the dominant one in high-quality Si *pn* junctions, it may not be dominant in low-quality junctions of Si or junctions of semiconductors with high E_g (therefore small n_i^2) such as GaAs. Often, another current called the *depletion-region-recombination* current is significant. This current results from the recombinations that occur within the depletion region. It can be shown (Grove, 1967) that this current

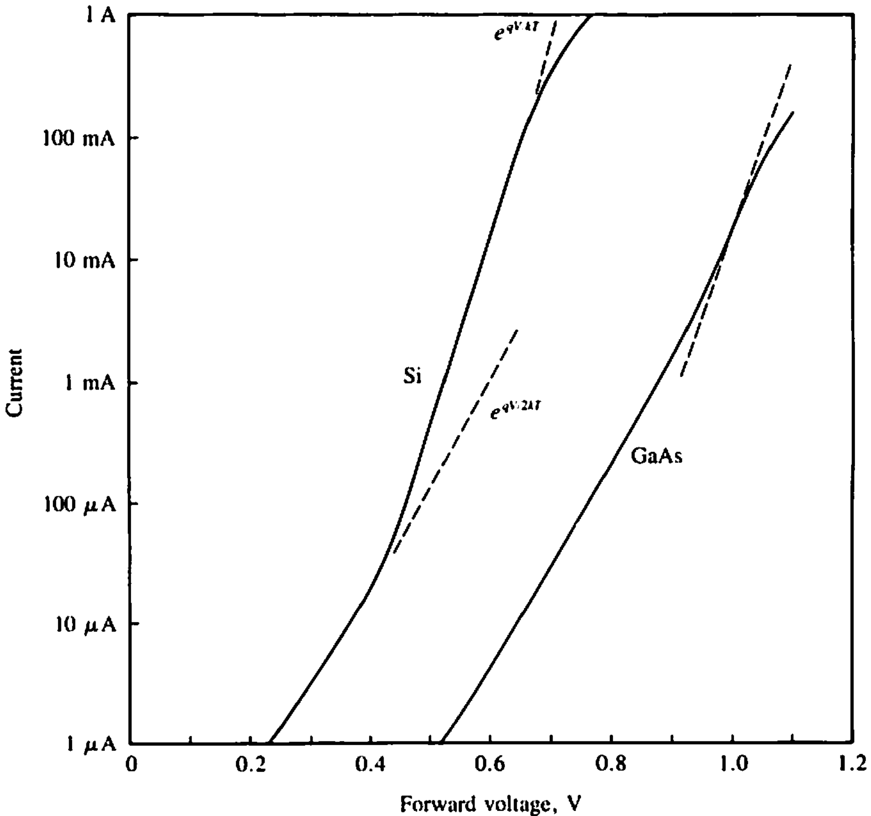

Figure 3.11 *I-V* characteristics of high-quality *pn* junctions at 25°C. Large area *pn* junctions typically show higher currents at the low voltage range.

density is

$$J_r \approx \frac{qn_i}{\tau_0} W e^{qV/2kT} \tag{3.5.14}$$

$$W = \sqrt{\frac{2\epsilon_s}{q}(V_d - V)\frac{N_a + N_d}{N_a N_d}} \tag{3.5.15}$$

ϵ_s is the permittivity of the semiconductor. Also, at high current levels, the so called *high-level-injection effect* invalidates Eq. (3.5.12) and makes J_{inj} follow a $e^{qV/2kT}$ relationship. Figure 3.11 shows some actual current-voltage curves and highlights the effects of temperature and bandgap energy. Often, over a current range the *I*-*V* characteristics may be fitted to

$$J = J_0(e^{qV/\gamma kT} - 1) \tag{3.5.16}$$

where γ is between 1 and 2 and J_0 and γ are determined by curve fitting. It will be seen later that good solar cell performance demands small J_0 and γ.

Figure 3.12 plots Eq. (3.5.16) on a linear current scale. Clearly, a *pn* junction passes large current in one direction only. Therefore, a *pn* junction is a *rectifying* junction. As a practical device, a *pn* junction is called a *rectifier* or a *diode*.

Many other types of junctions also exhibit the behavior represented by Eq. (3.5.16). They include certain metal/semiconductor or Schottky junctions, electrolyte/semiconductor junctions, and junctions between two dissimilar semiconductors such as Cu_2S and CdS. These junctions are interesting and attractive alternatives to *pn* junctions as solar cell structures. Any discussion of solar cells based on Eq. (3.5.16), then, applies to all types of solar cells and not just to *pn* junction solar cells.

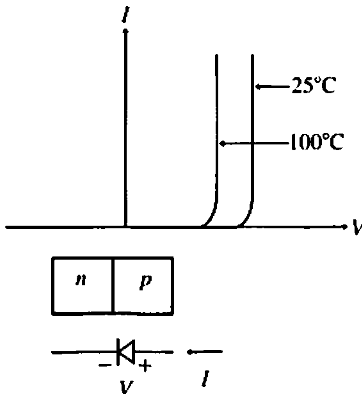

Figure 3.12 *I*-*V* characteristics and symbol of a rectifying diode.

3.6 SHORT-CIRCUIT CURRENT

In this section we analyze the diode current in the presence of light and introduce the important concept of the short-circuit current.

If the two terminals of a diode are connected through a conductor (short circuit), no current will flow in the circuit according to Eq. (3.5.16), since the diode voltage is zero. A delicate balance exists between the tendency of carrier flow by diffusion and the impeding effect of the potential barrier at the junction. The balance is tipped when light shines on a diode, as shown in Fig. 3.13. A current, aptly called the *short-circuit current*, I_{sc}, flows in the circuit from the p-side terminal to the n-side terminal.

The most convenient way of analyzing the short-circuit current is to divide the solar spectrum into many segments, each having a narrow range of wavelength, and find the current due to each spectral segment. Since each spectral segment is essentially monochromatic, it may be assigned a single wavelength λ and an absorption coefficient $\alpha(\lambda)$. If the number of incident photons in this spectral segment per square centimeter per second is $F(\lambda)$, the carrier-generation rate (cm^{-3} s^{-1}) [Eq. (3.3.3)] is

$$G(x) = \alpha F(1 - R)e^{-\alpha x} \tag{3.6.1}$$

where R is the reflectivity of the solar cell surface and is in general a function of λ. The minority carrier continuity equations are

$$\frac{dJ_n}{dx} - \frac{n_p - n_{p0}}{q\tau_n} + G(x) = 0 \qquad \text{for electrons in } p\text{-type material} \tag{3.6.2}$$

and

$$\frac{dJ_p}{dx} + \frac{p_n - p_{n0}}{q\tau_p} - G(x) = 0 \qquad \text{for holes in } n\text{-type material} \tag{3.6.3}$$

J_n and J_p are given in Eqs. (3.5.3) and (3.5.5). The boundary conditions,

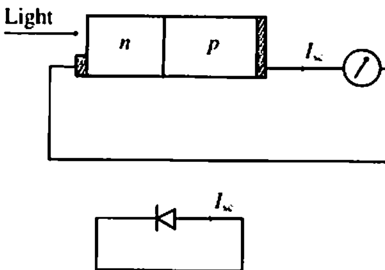

Figure 3.13 Schematic showing the direction of short-circuit current generated by light. The front layer (n-type in this illustration) is usually a diffused region; the p-region is the bulk or the base.

Eqs. (3.5.6) through (3.6.9), are applicable except that $V = 0$ (short circuit) in Eqs. (3.5.6) and (3.5.7). Again assuming zero electric fields outside the depletion region, the general solution to Eq. (3.6.3) is

$$p_n(x) - p_{n0} = A \cosh \frac{x}{L_p} + B \sinh \frac{x}{L_p} - \frac{\alpha F(1 - R)\tau_p}{\alpha^2 L_p^2 - 1} e^{-\alpha x} \qquad (3.6.4)$$

A and B can be determined from the boundary conditions and the resulting hole photocurrent at the junction, $x = x_j$, is

$$J_p = \left[\frac{qF(1 - R)\alpha L_p}{\alpha^2 L_p^2 - 1}\right] \left[\frac{\dfrac{S_p L_p}{D_p} + \alpha L_p - e^{-\alpha x_j}\left(\dfrac{S_p L_p}{D_p} \cosh \dfrac{x_j}{L_p} + \sinh \dfrac{x_j}{L_p}\right)}{\dfrac{S_p L_p}{D_p} \sinh \dfrac{x_j}{L_p} + \cosh \dfrac{x_j}{L_p}} - \alpha L_p e^{-\alpha x_j}\right] \qquad (3.6.5)$$

This is the photocurrent due to the holes generated in the top layer of a n/p (n on p) junction solar cell and collected by the junction. Similarly, Eq. (3.6.2) can be solved to yield the photocurrent due to electrons collected at the junction from the p layer behind the junction,

$$J_n = \frac{qF(1 - R)\alpha L_n}{\alpha^2 L_n^2 - 1} e^{-\alpha(x_j + W)} \times \left[\alpha L_n - \frac{\dfrac{S_n L_n}{D_n}\left(\cosh \dfrac{H'}{L_n} - e^{-\alpha H'}\right) + \sinh \dfrac{H'}{L_n} + \alpha L_n e^{-\alpha H'}}{\dfrac{S_n L_n}{D_n} \sinh \dfrac{H'}{L_n} + \cosh \dfrac{H'}{L_n}}\right] \qquad (3.6.6)$$

where x_j, W, H', and H are defined as in Fig. 3.10.

The electric field in the depletion region is so high that nearly all the light-generated carriers are swept out of the depletion region before they can recombine. The photocurrent due to the depletion region is therefore equal to the number of absorbed photons multiplied by q:

$$J_{dr} = qF(1 - R)e^{-\alpha x_j}(1 - e^{-\alpha W}) \qquad (3.6.7)$$

$$J_{sc}(\lambda) = J_n + J_p + J_{dr} \qquad (3.6.8)$$

W is given in Eq. (3.5.15). The total short-circuit photocurrent J_{sc} is the sum of Eqs. (3.6.5), (3.6.6), and (3.6.7). These three equations can be rewritten for p/n cells by interchanging the subscript n with subscript p. The short-circuit current is a function of the cell design and is proportional to the photon

flux. To isolate the effects of the internal cell design parameters, one often studies the spectral response of the cell

$$\mathrm{SR} \equiv \frac{J_{sc}(\lambda)}{qF(1 - R)} \tag{3.6.9}$$

This internal spectral response is simply the ratio of the number of collected carriers to the number of photons entering the cell. When the surface reflectivity is considered a cell design parameter, one also speaks of an *external* spectral response

$$\mathrm{SR}_{ext} \equiv \frac{J_{sc}(\lambda)}{qF} \tag{3.6.10}$$

Clearly SR is always greater than SR_{ext} and both are less than unity. The spectral response is also known as the *collection efficiency*, $\eta_{coll}(\lambda)$.

Figure 3.14 shows the calculated internal spectral response of several silicon solar cells. For wavelengths shorter than 4000 Å, photons are almost completely absorbed in the front n region. In this wavelength range, $\eta_{coll}(\lambda)$ is determined by x_j, s_p, and τ_p, which is assumed to be 3 ns. Between 5000

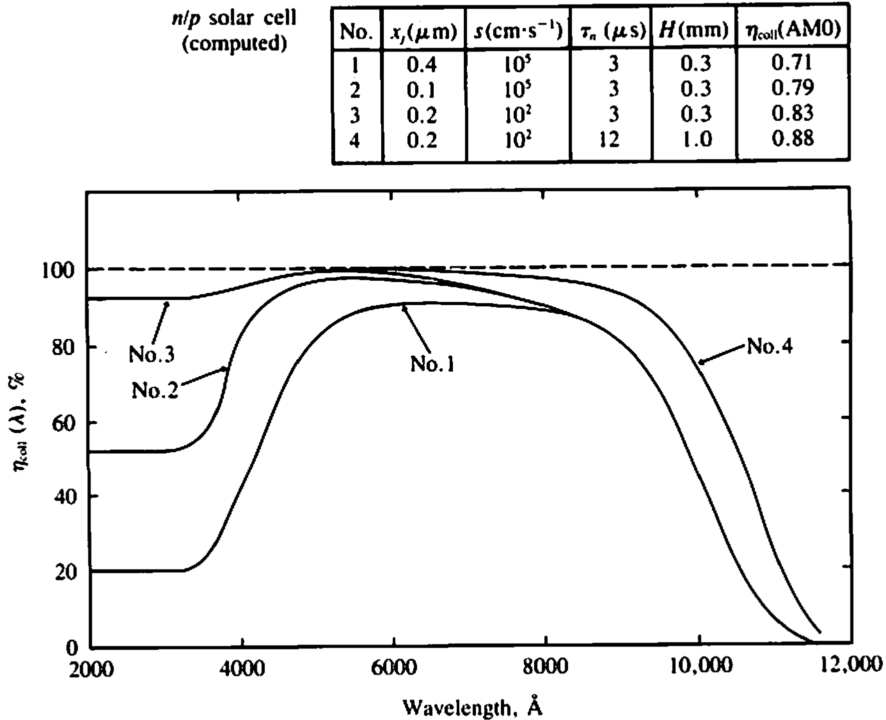
n/p solar cell (computed)

No.	$x_j(\mu m)$	$s(cm \cdot s^{-1})$	τ_n (μs)	H(mm)	η_{coll}(AM0)
1	0.4	10^5	3	0.3	0.71
2	0.1	10^5	3	0.3	0.79
3	0.2	10^2	3	0.3	0.83
4	0.2	10^2	12	1.0	0.88

Figure 3.14 Calculated internal spectral responses of Si solar cells. Assumptions: τ_p = 3 ns, $S_n \rightarrow \infty$. *(Wolf, 1971.)*

Å and 9000 Å, the bulk lifetime, τ_n and x_j are important. Most of the usable solar insolation falls in this spectral range. Beyond 9000 Å, photons have long penetration depths in Si. Therefore the cell thickness and the recombination velocity at the back surface, S_n, assumed to be infinite, are important.

The total cell short-circuit current is the sum of the contributions from all the spectral segments

$$J_{sc} = \sum_i qF(\lambda_i)[1 - R(\lambda_i)]\mathrm{SR}(\lambda_i) \tag{3.6.11}$$

The total collection efficiency is

$$\eta_{ext} = J_{sc}/q \sum_i F(\lambda_i) \tag{3.6.12}$$

$q\Sigma_i F(\lambda_i)$ is simply the maximum available short-circuit current (plotted in Fig. 3.6). Typical solar cells collect 60 to 90 percent of the maximum possible current.

3.7 EFFICIENCY

In Sec. 3.5 we have analyzed the diode current under voltage bias in the dark, and in Sec. 3.6, the diode current in the light without bias (short-circuit). When both light and voltage bias are present, the total diode current is the sum of I_{sc} and the dark diode current.

$$\begin{aligned} I(V) &= I_{sc} + \text{dark diode current as function of } V \\ &= I_{sc} - I_0[e^{(qV/\gamma kT)} - 1] \end{aligned} \tag{3.7.1}$$

following Eq. (3.5.16). Figure 3.15*a* illustrates this summation. If light intensity varies, I_{sc} varies and the *I-V* curve would move as a whole up and down in the figure. Figure 3.15*b* is the equivalent circuit of a solar cell. The output voltage and current of a solar cell is determined only when a load is connected to the solar cell. An ideal battery load, which has fixed terminal voltage, is assumed in Fig. 3.15*c*, while a resistive load is assumed in Fig. 3.15*d*. When the load is a short circuit ($V_{out} = 0$), I_{out} is simply I_{sc}. When the load is an open circuit ($I_{out} = 0$), the corresponding V_{out} is called the *open-circuit voltage*, V_{oc}. From Eq. (3.7.1)

$$V_{oc} = \frac{\gamma kT}{q} \ln\left(\frac{I_{sc}}{I_0} + 1\right) \tag{3.7.2}$$

The power output is

$$P_{out} = V_{out} \times I_{out} \tag{3.7.3}$$

By observation of the *I-V* curve, one expects that a particular pair of V_{out} and I_{out} called V_m and I_m will maximize P_{out}.

$$\max P_{out} \equiv P_m = V_m \times I_m \tag{3.7.4}$$

V_m can be found by substituting I_{out} in Eq. (3.7.3) with $I_{sc} - I_0 \times [e^{(qV_{out}/\gamma kT)} - 1]$, differentiating P_{out} with respect to V_{out} and setting the result equal to zero. Once V_m is known, I_m and P_m can be calculated. Depending on $qV_{oc}/\gamma kT$, V_m is typically 75 to 90 percent of V_{oc}, and I_m is typically 85 to 97 percent of I_{sc}. It is useful to define a *fill factor*,

$$\mathrm{FF} = \frac{P_m}{V_{oc} \times I_{sc}} \tag{3.7.5}$$

which is just the ratio of the area of the largest rectangle that can fit under the I-V curve to the product $V_{sc} \times I_{oc}$. The maximum possible power output can now be expressed as

$$P_m = V_{oc} \times I_{sc} \times \mathrm{FF} \tag{3.7.6}$$

FF is a function of $qV_{oc}/\gamma kT$, or $\ln [(I_{sc}/I_0) + 1]$ as shown in Fig. 3.16.

The power conversion efficiency of a solar cell is

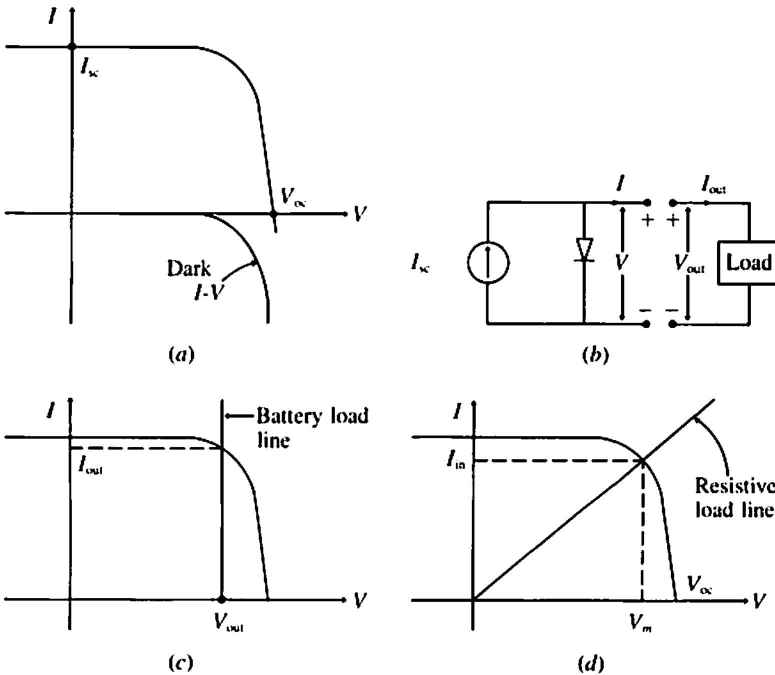

Figure 3.15 (*a*) By superposition, I_{sc} plus the dark current yields the I-V curve of a solar cell. (*b*) Cell I-V curve and load determine the output current and voltage. (*c*) An ideal battery load. (*d*) A resistance load.

LIGHT SENSORS; PHOTODIODES AND PHOTOCONDUCTORS

Referring to Fig. 3.15*a*, a short-circuited or reverse-biased diode (negative V) passes no (or negligible) current in the dark, and in the light passes I_{sc}, which is proportional to the light intensity. By measuring the reverse current one can gauge the light intensity. When used in this fashion the device is called a *photodiode*.

Photodiodes, often made of silicon, are used, for example, as the detectors or receivers in the emerging fiber-optical communication systems. In such systems, signals are transmitted as variations in light intensity through glass fibers as thin as human hair. The glass is of such clarity that light is attenuated by as little as 10 percent in traveling through a 1-km length of the fiber.

Another common type of light sensor is the photoconductor. Photo-carrier generation increases the electron and hole densities in a semiconductor and thus increases its conductivity (see Eq. 3.5.7). By measuring the conductance change (change of current under constant applied voltage), one can sense the light intensity. CdS photoconductor sensors are widely used in the exposure systems of cameras. Unlike Si, CdS does not respond to infrared light and thus matches human eyes more closely.

$$\eta \equiv \frac{P_m}{P_{in}} = \frac{V_{oc} \times I_{sc} \times \text{FF}}{\text{incident solar power}} \tag{3.7.7}$$

In order to achieve high conversion efficiency, it is clearly desirable to have

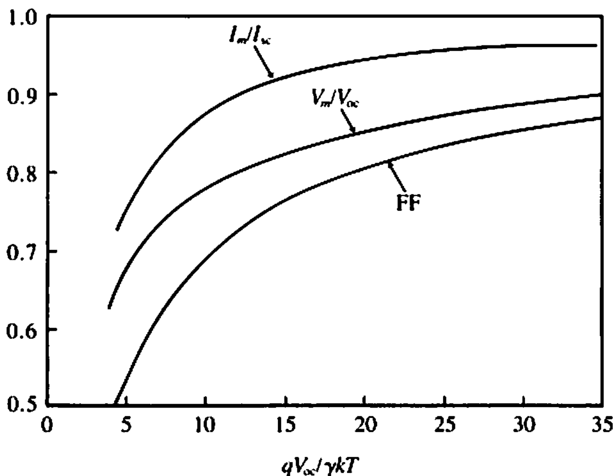

Figure 3.16 V_m/V_{oc}, I_m/I_{sc}, and FF as functions of $qV_{oc}/\gamma kT$. Note that $qV_{oc}/\gamma kT = \ln(I_{sc}/I_0 + 1)$.

high I_{sc} or high collection efficiency, high V_{oc} or low dark current, and high fill factor or a sharp corner in the *I-V* curve.

Present-day Si solar cells have efficiencies between 12 and 17 percent under one sun (AM1) illumination. Figure 3.17 is an accounting sheet of the energy losses (Wolf, 1971). In the solar spectrum, 26 percent of the energy is in the photons having $h\nu < 1.1$ eV. Of the remaining useful photons, most have energy much larger than 1.1 eV. The excess energy is wasted since there is no difference between the electron–hole pairs generated by a 1.1-eV photon and by a 2.5-eV photon. Forty-one percent of the energy in photons is so wasted. Even an ideal cell can only turn the remaining $0.78 \times 0.59 = 0.44$ or 44 percent into electricity. Depending on the cell design and the material parameters, real cells have efficiencies between 12 and 17 percent.

3.8 FACTORS AFFECTING THE CONVERSION EFFIENCY

Bandgap Energy

The relationship between V_{oc} and E_g can be illustrated by assuming that I_{inj} in Eq. (3.5.12) is the dominant diode current

$$V_{oc} \approx \frac{kT}{q} \ln \frac{J_{sc}}{J_0} \tag{3.8.1}$$

From Eqs. (3.5.13) and (3.2.1)

$$\begin{aligned} J_0 &= n_i^2 \left(\frac{C_p}{N_d} + \frac{C_n}{N_a} \right) \\ &= Be^{-E_g/kT} \left(\frac{C_p}{N_d} + \frac{C_n}{N_a} \right) \end{aligned} \tag{3.8.2}$$

where the definitions of C_p and C_n are obvious from Eq. (3.5.13). Substituting (3.8.2) into (3.8.1)

$$V_{oc} \approx \frac{E_g}{q} - \frac{kT}{q} \ln \left[\frac{B}{J_{sc}} \left(\frac{C_p}{N_d} + \frac{C_n}{N_a} \right) \right] \tag{3.8.3}$$

Since it is logarithmic, the second term in Eq. (3.8.3) is more or less a constant and is typically 0.5 V. Thus, Si has $E_g = 1.12$ eV and silicon solar cells have $V_{oc} \approx 0.55$ V; GaAs has $E_g = 1.43$ eV and GaAs solar cells have $V_{oc} \approx 0.9$ V.

V_{oc} increases with increasing E_g. On the other hand, in Fig. 3.7 we have seen that the maximum possible J_{sc} decreases with increasing E_g. As a result, we may expect solar cell efficiency to peak at a certain E_g. This is borne out by Fig. 3.18, which plots calculated conversion efficiencies for unity collection efficiency, 10^{17} cm^{-3} doping concentration and typical lifetimes.

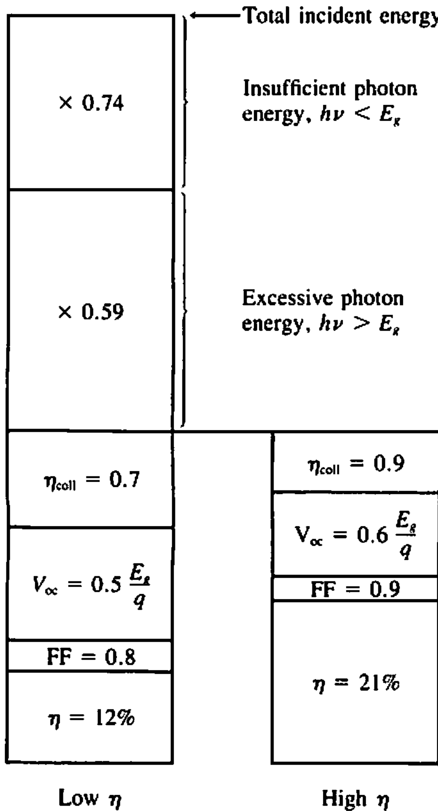

Figure 3.17 Accounting of the energy losses in a typical low efficiency and a hypothetical, very high efficiency, Si solar cell.

It is worth noting that the "maximum" efficiencies shown in Fig. 3.18 can be exceeded in concentrator systems (see Chap. 5) and in systems where several solar cell materials (see Chap. 12) or materials having graded bandgaps (see Chap. 11) are employed.

Temperature

Figure 3.18 also shows that η decreases with increasing temperature. A reading of Sec. 3.6 would show that I_{sc} is insensitive to T. It is V_{oc} that is responsible for the temperature dependence. From Eq. (3.8.3)

$$\frac{dV_{oc}}{dT} = \frac{1}{q}\frac{dE_g}{dT} - \frac{k}{q}\ln\left[\frac{B}{J_{sc}}\left(\frac{C_p}{N_d} + \frac{C_n}{N_a}\right)\right]$$

$$= \frac{1}{q}\frac{dE_g}{dT} - \frac{1}{T}\left(\frac{E_g}{q} - V_{oc}\right) \tag{3.8.4}$$

For Si, $dE_g/dT = -0.0003$ eV/°C, $E_g/q - V_{oc} \approx 0.5$ V, therefore

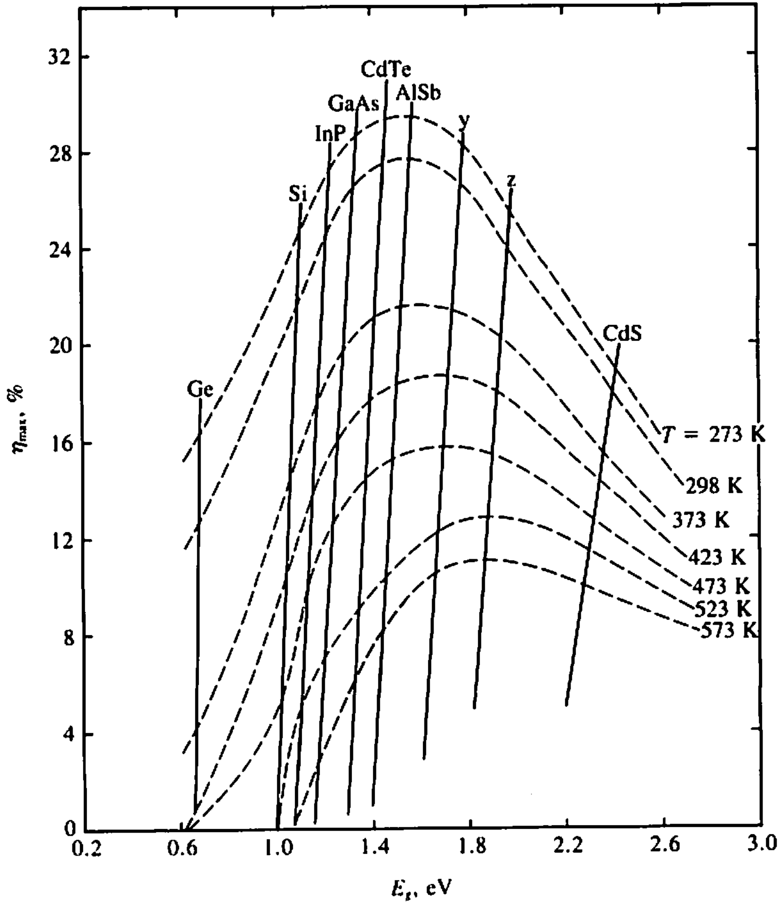

Figure 3.18 Calculated upper limits of efficiency. Assumptions: Unity collection efficiency, 10^{17} cm^{-3} doping, typical lifetimes. These limits may be exceeded by using light concentration or employing more than one solar cell material. *(Rappaport, 1959.)*

dV_{oc}/dT = −2 mV/°C. For every 1°C increase in temperature, V_{oc} drops by about 0.002/0.55 ≈ 0.4% of its room temperature value, and hence η drops by about the same percentage. For example, a Si cell having 20% efficiency at 20°C will only be about 12% efficient at 120°C. For GaAs, V_{oc} drops by 1.7 mV or 0.2% per °C. These calculated values agree well with measured temperature sensitivities. In Eq. (3.8.4), the dE_g/dT term can usually be neglected. dV_{oc}/dT, then, can be predicted from the knowledge of E_g and V_{oc} of any given cell.

Recombination Lifetime

Long carrier-recombination lifetimes are desirable mainly because they help achieve large I_{sc}. In indirect-gap materials such as Si, significant numbers of carriers are generated as far as 100 μm from the junction, and recombination lifetimes longer than 1 μs are desirable. In direct-gap materials such as GaAs or Cu_2S, recombination lifetimes as short as 10 ns may suffice. Long lifetimes also reduce the dark current and increase V_{oc}.

The key to achieving long recombination lifetimes is to avoid introducing recombination centers during material preparation and cell fabrication. Proper but often elusive "gettering" steps in the fabrication process can improve lifetimes by removing the recombination centers.

Light Intensity

In Chap. 5 we shall discuss the concept of focusing sunlight on solar cells so that a small solar cell can produce a large amount of electric power. Assuming that the sunlight intensity is concentrated by X times, the input power per cell area and J_{sc} both increase by X times. V_{oc}, according to Eq. (3.8.3), also increases by (kT/q) ln X, e.g., 0.12 V for $X = 100$. The output power therefore increases by more than X times and the conversion efficiency is higher as a result of sunlight concentration.

Doping Density and Profile

Another factor that can have a significant effect on V_{oc} is the doping density. Although N_d and N_a appear in the logarithmic term in Eq. (3.8.3) they can also be easily changed by orders of magnitude. The higher the doping densities, the higher is V_{oc}. A phenomenon known as the *heavy doping effect* has recently received much attention. Because of the deformation of the band structure and the change in electron statistics at high doping concentrations, N_d and N_a in all the equations should be replaced by $(N_d)_{eff}$ and $(N_a)_{eff}$, which are shown in Fig. 3.19*a*. Since $(N_d)_{eff}$ and $(N_a)_{eff}$ exhibit peaks, it may not be advantageous to use very high N_d and N_a, particularly since the lifetimes tend to decrease at high doping densities, probably due to Auger recombination as discussed in Sec. 3.4. Figure 3.19*b* illustrates this point.

At the present time, the base doping density is usually about 10^{16} cm^{-3} in Si solar cells and about 10^{17} cm^{-3} in cells of direct-gap materials. The front diffused region is usually doped to higher than 10^{19} cm^{-3} in order to minimize the series resistance, which will be discussed later. The heavy doping effect is thus more important in the diffused region.

When N_a and N_d, or better, $(N_a)_{eff}$ and $(N_d)_{eff}$, are not uniform but decrease

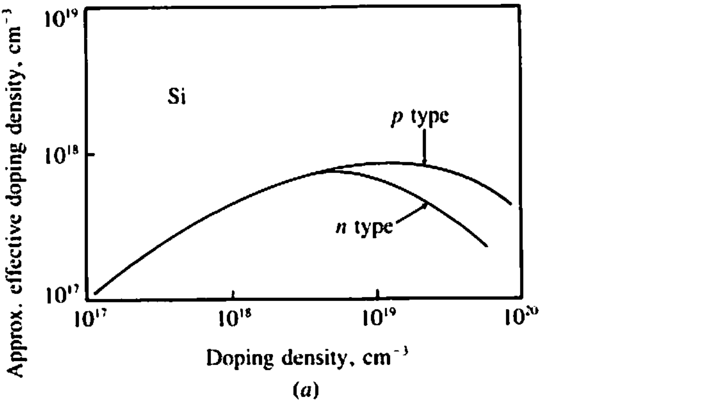

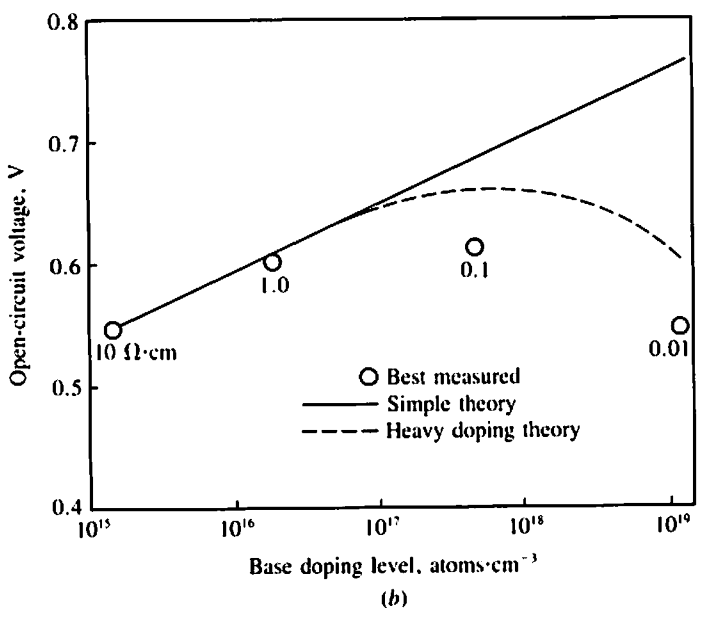

Figure 3.19 (*a*) The high doping effect: The effective doping density saturates or even drops with increasing doping density.
(*b*) V_{oc} as a function of the bulk doping density. *(Godlewski et al., 1977.)*

toward the junction, electric fields are set up in such directions as to aid the collection of photo-generated carriers. These fields improve I_{sc}. Such non-uniform doping profiles are usually impractical in the base region of the cell. They are natural in the diffused region—provided that attention is paid to the heavy doping effect.

Surface Recombination Velocities

Low surface recombination velocities help enhance I_{sc}. They also improve V_{oc} by reducing I_0. The recombination velocity at the front surface is difficult to measure and is often assumed to be infinite (a perfect trap of carriers). If the back of the cell is alloyed to a metal contact, the recombination velocity at the back surface would also be infinite. In recent years, however, a design called the *back-surface field* (BSF) cell (Mandelkorn et al., 1973) has become popular. Figure 3.20 shows the structure. An additional p^+ layer is diffused into the back side of the cell before the metal contact is deposited. As the energy diagram in Fig. 3.20 shows, the p/p^+ interface presents a barrier to the electrons that would have easily reached the ohmic contact and recombined there. It can be shown that the recombination velocity at the p/p^+ interface, which is now considered the back surface for evaluating Eqs. (3.5.13) and (3.6.6), can be expressed as (Hauser, 1975)

$$S_n = \frac{N_a}{N_{a^+}} \frac{D_{n^+}}{L_{n^+}} \coth \frac{W_{p^+}}{L_{n^+}} \qquad (3.8.5)$$

where N_{a^+}, D_{n^+}, and L_{n^+} are the doping density, diffusion coefficient, and diffusion length in the p^+ region. If $W_{p^+} = 0$, then $S_n = \infty$ as expected. However, if W_{p^+} is comparable to L_{n^+} and $N_{a^+} >> N_a$, then S_n can be assumed to be zero. The effects of S_n on J_{sc}, V_{oc}, and η are illustrated in Fig. 3.21. Note that both J_{sc} and η show a peak when S_n is small.

Series Resistance

In any real solar cell there is some series resistance, which can arise from the lead, the metal contact grid, or the bulk cell resistance. However, the domi-

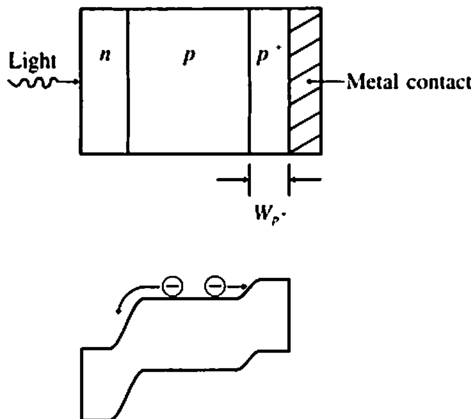

Figure 3.20 Back surface field cell. The field at the p/p^+ junction retards the flow of the electrons toward the back surface.

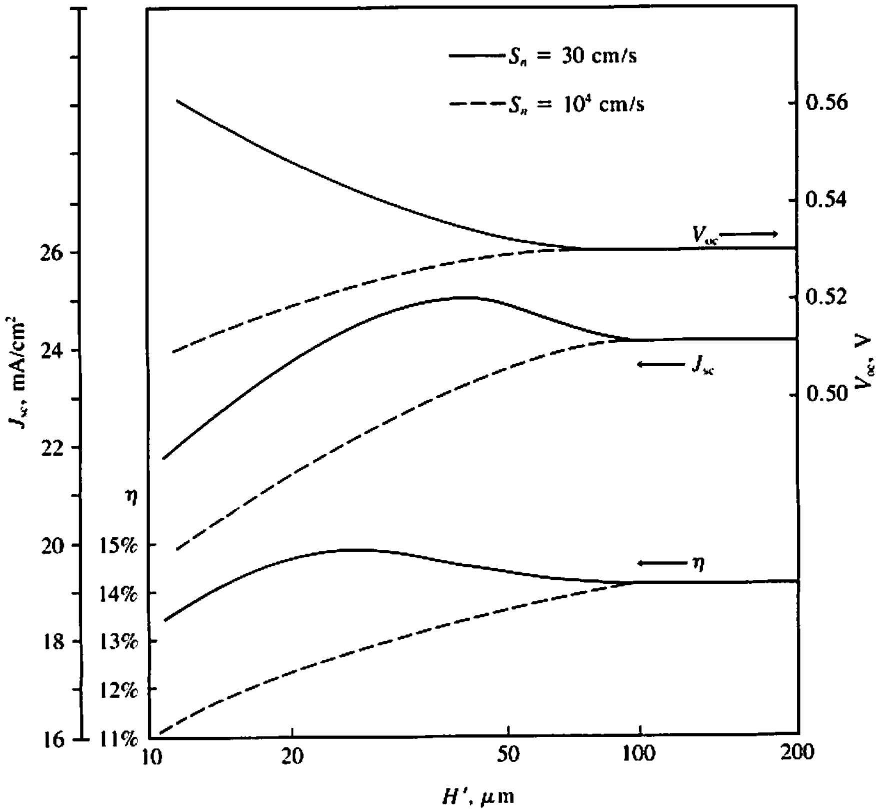

Figure 3.21 Effects of the back surface recombination velocity on cell performance. Note that η peaks at certain cell thicknesses when S_n is small.

nant source of series resistance is usually the thin diffused layer. Current collected at the *pn* junction in Fig. 3.1 must flow in the *n* layer to the closest metal line, and this is a resistive path. Clearly, the series resistance can be minimized by spacing the metal lines closely.

The effect of a finite series resistance, R_s is to shift the *I*-*V* curve in, say, Fig. 3.15*d* to the left by $I \times R_s$. Roughly speaking, this has the effect of reducing V_m by $I_m \times R_s$. If $I_m \times R_s << V_m$, the impact on η is minimal. This is usually the case except when the material has very high resistivity, such as with many amorphous and organic semiconductors, or when I_m is large, as in a concentrator system.

Metal Grid and Optical Reflection

The metal contact grid on the front surface is opaque to sunlight. To maximize I_{sc}, the area occupied by the metal grid should be minimized. In order to keep

R_s low, the general rule is to make the metal grid in the form of closely spaced, fine lines.

Not all the light can enter Si because of optical reflection. The reflectivity of a bare Si surface is about 40 percent. It can be reduced by the use of antireflection coatings. For a single-frequency light incident on the cell at a right angle, the reflectivity can be made zero by a single coating one-fourth wavelength thick and having an index of refraction equal to $\sqrt{n}$, where n is the index of refraction of Si. More than 90 percent of the usable photons in the solar spectrum can be transmitted into Si when a 600-Å coating of Ta_2O_5 is applied; 84 percent is transmitted with a 1000-Å coating of SiO_2. Better results can be achieved with multiple-layer coatings (Wang et al., 1973). Less is transmitted when light is incident at an oblique angle.

3.9 SUMMARY

Many structures, such as *pn* junctions and metal-semiconductor junctions, exhibit a distinctive rectifying *I-V* characteristic as shown in Fig. 3.12. Under illumination, their *I-V* curves are shifted parallel to the current axis as shown in Fig. 3.15*a*. Connected to a load, the device would operate in the quadrant of positive voltage and positive current (Fig. 3.15), thus providing power to the load.

The conversion efficiency of a solar cell is the ratio of its output electrical power to the input light power. To achieve high efficiency, it is desirable to have large short-circuit current, high open-circuit voltage, and large fill factor. The short-circuit current is higher if the solar cell is made from materials with small energy gap, E_g. Good fabrication processes and good cell design can also increase the short-circuit current by minimizing carrier recombination. Solar cells made of material having a large E_g tend to have higher open-circuit voltage. Fill factor is a measure of the sharpness of the knee in the *I-V* curve. It can be lowered by the presence of series resistance and tends to be higher whenever the open-circuit voltage is higher. The conversion efficiency increases with increasing light intensity and decreasing temperature.

The highest efficiencies are expected from solar cells made from materials with E_g between 1.2 and 1.6 eV. For thin-film cells, direct-gap semiconductors, which absorb photons near the surface, are preferable. The most common solar cells, silicon *pn*-junction cells, have efficiencies ranging between 12 and 17 percent.

REFERENCES

Godlewski, M. P., Brandhorst, H. W., Barona, C. R. (1977), Record, 12th IEEE Photovoltaic Spec. Conf., 32–36.

Grove, A. S. (1967), *Physics and Technology of Semiconductor Devices*, John Wiley & Sons.
Gutmann, F., and Lyons, L. E. (1967), *Organic Semiconductors*, John Wiley & Sons.
Hauser, J. R. and Dunbar, P. M. (1975), *Solid State Elec.*, Vol. 18, 715.
Hovel, H. J. (1975), *Semiconductors and Semimetals, Vol. 11—Solar Cells*, Academic Press.
Mandelkorn, J., Lamneck, J. H., and Scudder, L. R. (1973), Record, 10th IEEE Photovoltaic Spec. Conf., 207–211.
Muller, R. S. and Kamins, T. (1977), *Device Electronics for Integrated Circuits*, Wiley-Interscience.
Rappaport, P. (1959), *RCA Rev.*, Vol. 20, September, 373–397.
Varshni, Y. P. (1967), *Phys. Stat. Sol.*, Vol. 19, 459–514.
Wang, E. Y., Yu, F. T. S., and Sims, V. L. (1973), Record, 10th IEEE Photovoltaic Spec. Conf., 168–173.
Wolf, M. (1971), *Energy Conversion*, Vol. 11, June, 63–73.

PROBLEMS

3.1 *Solar cell current versus bandgap* What is the relationship between the left- and right-hand vertical scales of Fig. 3.5? In your own words explain why cells made of narrow bandgap materials may be expected to generate more current.

3.2 *Simiplification of diode current expression*

(*a*) Find the expression for J_0 (3.5.13) in the limiting case of $S_p = S_n = \infty$.

(*b*) Further simplify the expression by assuming $X_j >> L_p$ and $H' >> L_n$. The resultant expression should be familiar if you have studied the theory of *pn* junctions.

3.3 *Derivation of solar cell I-V expression*

(*a*) Show that Eq. (3.6.4) satisfies Eq. (3.6.3).

(*b*) Find A and B in Eq. (3.6.4) from the boundary conditions.

(*c*) Using the results of (*b*), verify Eq. (3.6.5).

3.4 *Cell efficiency* In your own words, discuss Fig. 3.14.

3.5 *Calculation of cell efficiency* Assuming that a Si solar cell has $J_{sc} = 35$ mA/cm^2 under AM1, from Fig. 3.5 find η_{coll}. Assuming that its $J_0 = 10^{-11}$ mA/cm^2, find V_{oc} and FF from Fig. 3.16 and its caption. Finally, follow the example of Fig. 3.17 to find the efficiency of this cell. Note that η can be found more directly from $P_{out} = J_{sc} \times V_{oc} \times$ FF and the AM1 radiation intensity given in Chap. 2. Try it.

3.6 *Temperature effects* Derive Eq. (3.8.4). Using the information in Fig. 3.18, plot two curves of η versus T for Si and GaAs, respectively. Compare them with the discussion in the text following Eq. (3.8.4).

3.7 *Factors affecting cell efficiency* Are J_{sc}, V_{oc}, and η improved, degraded, or not significantly affected when each of the following is increased: T, τ, E_g, S, sunlight concentration ratio, N_a and N_p, cell thickness, series resistance, cell reflectance?

CHAPTER

FOUR

MATERIALS AND PROCESSING

CHAPTER OUTLINE

4.1 MATERIAL PROPERTIES AND PROCESSING TECHNIQUES
BOX: MAKING AN INTEGRATED CIRCUIT
4.2 CONVENTIONAL SILICON CELL PROCESSING
4.3 PROCESSING CADMIUM SULFIDE CELLS
4.4 ENVIRONMENTAL AND OTHER CONSIDERATIONS
4.5 SUMMARY
REFERENCES
PROBLEMS

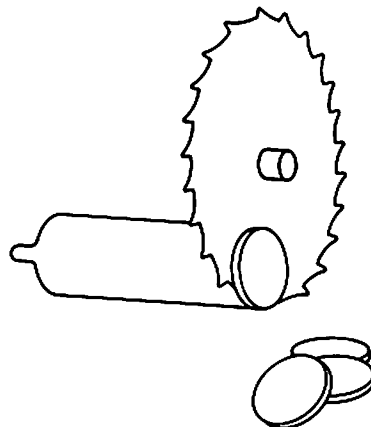

Terrestrial solar cells made conventionally from single-crystal silicon are constructed as shown in Fig. 4.1. Typical *n*-on-*p* cells have been made from round silicon wafers about 0.3 mm thick. The unilluminated bottom, or back, side of a cell has a metal coating that contacts the *p*-type body of the silicon. An *n*-type top layer which forms the *pn* junction is heavily doped for low resistivity. Metal fingers about 0.1 mm wide and 0.05 mm thick make ohmic contact to this front layer to collect the current. A transparent insulating antireflection coating approximately 0.06 microns (μm) thick covers the top silicon layer and provides much better transmission of light than can be obtained with bare silicon.

Comparing this structure with that of an integrated circuit (IC), one is struck with the relative simplicity of the solar cell. The integrated circuit contains thousands of *pn* junctions in its transistors. The major features of it are only a few microns across, and the operations it performs are quite varied and complex when compared with those of the solar cell. Silicon fabrication techniques are well understood, and the processes used to make an integrated circuit can be used to make a solar cell as well. The reader may wonder why an entire chapter should be devoted to solar cell materials and processing.

4.1 MATERIAL PROPERTIES AND PROCESSING TECHNIQUES

It is true that silicon cells have been made for terrestrial applications by employing the conventional cell design and traditional IC processing methods. These have been relatively expensive cells, however, costing more than

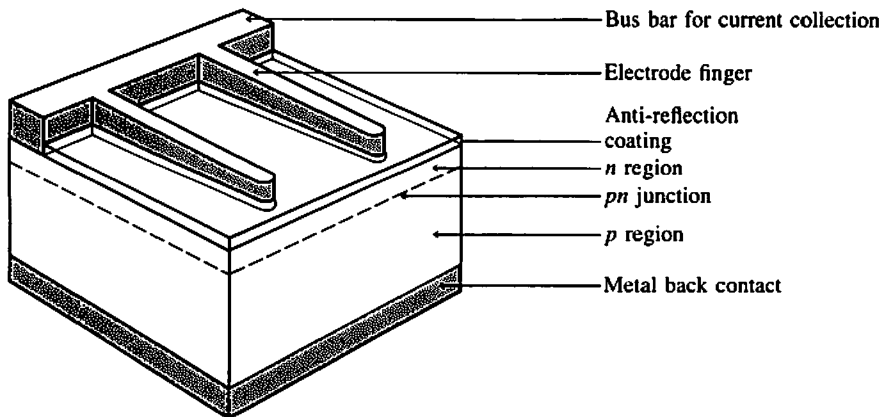

Figure 4.1 Schematic view of typical commercial single-crystal silicon solar cell.

MAKING AN INTEGRATED CIRCUIT

To create the thousands of transistors in an integrated circuit requires forming in a silicon wafer precisely dimensioned *n*-type and *p*-type regions containing different impurity atoms. The typical steps illustrated below to make a single *pn* junction in *p*-type silicon may be repeated several times during the manufacture of a complete integrated circuit.

One begins by entering in a computer file the precise locations of all the *n*-type regions in the circuit. The computer then controls an electron beam that draws the pattern by selectively exposing a film of electronresist (similar to photoresist described below). By chemical etching, the pattern of electronresist is transfered to an underlying thin chromium film on a glass plate. The glass plate carrying the chromium pattern (called a *photomask*) is slightly larger than the silicon water, whose diameter may range from 5 to more than 12 cm.

The surface of the silicon wafer is oxidized in a furnace heated to about 1000°C and having dry oxygen or steam flowing through it. One then makes openings in this oxide to permit dopant atoms to enter the silicon. The openings are made by first coating the oxide with a liquid photosensitive polymer, called *photoresist*, which is then hardened by baking and exposed with ultraviolet light through the photomask [sketch (*a*)]. Where the light reaches the photoresist, the polymer crosslinks strongly so that when the wafer is placed in a bath of developer the portions of the resist that were illuminated continue to adhere to the oxide. The resist washes away from each shaded region such as that under the dark line in the pattern, leaving openings through which the underlying oxide can be removed in a chemical bath or in a dry-plasma-etching process.

The remaining photoresist is then removed and [sketch (*b*)] dopant atoms enter the silicon through the opening in the oxide to change the silicon there to

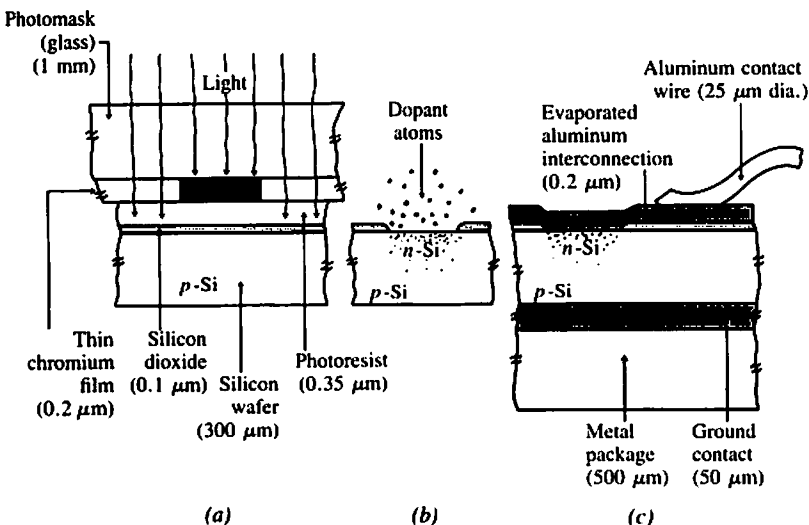

(*a*) (*b*) (*c*)

n-type. This doping may be done in a 1000°C furnace in which a gas containing phosphorus is flowing. Alternatively one may implant phosphorus ions accelerated in a vacuum to energies from tens to hundreds of thousands of electron-volts. After the implantation, a thermal annealing process eliminates structural damage and activates the dopant atoms so they produce mobile charge carriers.

These steps are repeated many times to make multiply doped and electrically connected regions that form the circuit. Additional layers of insulating oxides, and perhaps polycrystalline silicon, may be formed and patterned with other photomasks. Finally, an aluminum conductive layer is evaporated and patterned with yet another photoresist layer [sketch (*c*)]. The 0.4-cm-square circuit chips are now separated mechanically and put in individual packages. Connecting wires are attached to the accessible aluminum "pads" by ultrasonic bonding, and the circuit is ready for testing and use.

10 dollars per peak watt of output, and so have been most suitable for remote uses such as powering isolated communication equipment located where the cost of electricity from other sources is high. Two key factors affect the choices of cell materials and processing methods:

- *Cost of electrical energy produced.* The cost of output from a photovoltaic system—for example, in dollars per kWh—is determined by cell and array efficiencies, and all the costs incurred while fabricating, installing, and operating the system. To these must be added balance-of-system (BOS) costs, such as the cost of the land devoted to the system, and the cost of power conditioning and energy storage.
- *Energy payback time, or ratio.* Energy is used at each stage in the manufacture of a photovoltaic power system—in extracting the raw materials from the ground, in refining, in shaping the materials, and so on. The length of time that the system must operate to produce electrical energy equal to the total energy used in its manufacture, called the *energy payback time*, should be no more than a few years.

The *energy payback ratio*, the total energy produced during its useful life divided by the total energy used to make the system, must be greater than unity if the system is to be a net producer of energy. In an ideal free economic system, the energy payback performance of a solar cell system or any other power plant would be adequately reflected in the cost of the system. In actuality, it is necessary for technologists and policy makers to consider the energy payback separately from the cost of energy produced whenever the government regulates or subsidizes some components of the energy industry.

When comparing different photovoltaic systems, one may consider their relative *tolerance to ambient conditions*, such as temperature, moisture in the